Betatron oscillations of electrons accelerated in laser wakefields characterized by spectral x-ray analysis

Félicie Albert, Rahul Shah, Kim Ta Phuoc, Romuald Fitour, Fréderic Burgy, Jean-Philippe Rousseau, Amar Tafzi, Denis Douillet, Thierry Lefrou, and Antoine Rousse

Laboratoire d'Optique Appliquée, ENSTA, CNRS UMR7639, Ecole Polytechnique, Chemin de la Hunière, 91761 Palaiseau, France

(Received 27 July 2006; revised manuscript received 18 February 2008; published 7 May 2008)

Relativistic electrons accelerated by laser wakefields can produce x-ray beams from their motion in plasma termed betatron oscillations. Detailed spectral characterization is presented in which the amplitude of the betatron oscillations r is studied by numerical analysis of electron and x-ray spectra measured simultaneously. We find that r reaches as low as 1 μm in agreement with previous studies of radiation based on coherence and far-field spatial profile.

DOI: 10.1103/PhysRevE.77.056402 PACS number(s): 52.38.Ph, 52.25.Os, 52.50.Dg

I. INTRODUCTION

It has been many years since laser created plasmas have been proposed to accelerate electrons [1]. Their interest mainly relies on the fact that plasmas can produce large acceleration gradients, on the order of 100 GV/m compared to 100 MV/m for conventional radio-frequency linear accelerators [2]. Both three dimensional particle-in-cell simulations [3] and experiments have shown that it is possible to generate electron beams with energies up to GeVs. More recently, beams of quasimonoenergetic electrons have been measured from 70 MeV to a few hundred MeV [4–8]. An important application of these energetic particles is the production of x-ray radiation. In a synchrotron, GeV electron beams are injected in permanent magnet undulators with periodicities of a few centimeters to a few millimeters to produce x rays. Since the energy of laser-produced plasma electrons is in the sub-GeV range, the x-ray spectral domain cannot be achieved with such undulators. Much shorter periods are required in that case. To do so, we have recently demonstrated [9,10] that the laser-wakefield plasma itself can act as a wiggler (submillimeter oscillation periods). When an ultraintense laser is focused into a gas jet, the ponderomotive force plows the electrons away from the strong field regions leaving an ion cavity almost free of background electrons in its wake [3,11]. Electrons trapped in the ion cavity feel simultaneously the longitudinal and transversal electrostatic fields due to the space charge separation. During the acceleration by the longitudinal field to relativistic energies, the electrons acquire a transversal momentum due to the transverse field. They oscillate across the central axis of the ion cavity in the direction of propagation (betatron oscillation) [12–14] and a collimated beam of keV x-ray radiation is produced from this relativistic motion.

Following the first observation of betatron x-ray beams [9,10], recent works have shown that electrons accelerated in a petawatt-laser-generated plasma cavity produces as well this type of radiation [15] and that electron trajectories can be imaged and characterized from the spatial properties of the x-ray radiation [16,17]. Fresnel diffraction using knife-edge imaging of the x-ray source has shown that the maximum excursion of the electrons during their oscillation in the ion channel is below 4 μm [17]. Higher resolution in the electron motion analysis was obtained with the study of the far field structure of the x-ray beam and showed that electrons can follow similar trajectories with a transverse excursion close to the micrometer [16].

Here, we present the spectral analysis of the betatron process, and provide an accurate measurement of the betatron x-ray spectrum. We study the plasma wiggler parameters from the correlation between the electron and betatron x-ray beams by recording simultaneously their spectral properties. The paper is organized as follows: Sec. II presents the experimental and numerical methods used to analyze the experimental data and determine the plasma wiggler parameters; Sec. III describes the experimental setup as well as the experimental properties of the electron and x-ray beams. The betatron amplitude r is then characterized from x-ray spectral measurements in Sec. IV. Conclusion and perspectives are discussed in Sec. V.

II. METHODS FOR PLASMA WIGGLER CHARACTERIZATION

The plasma wiggler consists of an ion cavity where the charge separation is at the origin of the forces driving the motion of the electron. The electron is submitted to a longitudinal accelerating field and to a transverse field with cylindrical symmetry around the cavity axis. The oscillation motion has been described by the equation

$$\frac{d\vec{p}}{dt} = -m\omega_p^2 \vec{r}_\perp/2 + mc\omega_p \vec{u}_z, \tag{1}$$

where p is the relativistic momentum of the electron, m is the electron mass, $\vec{r}_\perp$ is the transverse position of the electron, and $\omega_p = (n_e e^2/m\epsilon_0)^{1/2}$ is the plasma frequency, with n_e the plasma electron density, e the electron charge, and $\vec{u}_z$ the unit vector in the channel axis direction z.

For small amplitude oscillations, the electron has a harmonic motion at the fundamental betatron frequency

$$\omega_\beta = \omega_p/\sqrt{2\gamma}, \tag{2}$$

where γ is the relativistic Lorentz factor of the electron. Due to its relativistic motion, the electron emits synchrotron radiation [13,14] at the fundamental wavelength $\lambda = \lambda_\beta/2\gamma^2$

where λ_β is the period of the betatron oscillation.

High harmonics are radiated in the forward direction and within a cone of divergence $\theta \simeq K/\gamma$ in the case of high amplitude oscillations in the wiggler of strength parameter K:

$$K = 1.33 \times 10^{-10}\sqrt{\gamma n_e(\mathrm{cm}^{-3})}\, r(\mu\mathrm{m}). \tag{3}$$

The radiation consists of a broadband spectrum if K becomes large ($K \gg 1$), and the spectral intensity $\frac{dI}{d\omega}$ can be described by the synchrotron radiation function [18,19]:

$$\frac{dI}{d\omega} = \frac{1}{4\pi\epsilon_0}\sqrt{3\pi/c}\frac{e^2}{c}\gamma\frac{\omega}{\omega_c}\int_{\omega/\omega_c}^{\infty} K_{5/3}(x)dx, \tag{4}$$

where ω_c represents the cutoff frequency, and $K_{5/3}$ is a modified form of the Bessel function. The x-ray intensity per spectral bandwidth increases up to $\omega_{pk} \simeq 0.29\omega_c$, and then drops exponentially to zero [18]. The cutoff frequency is [14] given by

$$\hbar\omega_c \simeq 5 \times 10^{-24}\gamma^2 n_e(\mathrm{cm}^{-3}) r(\mu\mathrm{m})\mathrm{keV}. \tag{5}$$

We have used a test particle model to describe both the electron orbits and the features of the betatron radiation. This simple model can properly represent the electron dynamics in the plasma cavity [10,12,14–17] for our experimental conditions. In the code we integrate the equation of motion and calculate the resulting synchrotron emission. The initial conditions are the electron plasma density, the transverse position $r=r_0$, and the momentum of the electron p_0 along the z channel axis at the trapping position in the wakefield cavity [initial energy $E_0(\mathrm{MeV}) = \sqrt{(1+p_0^2)}/2$ with p_0 normalized to mc]. The ion cavity is centered on the laser propagation axis ($r=0$), where the transverse field is zero. The fields used in the equation of motion [Eq. (1)] depend on the plasma electronic density and r. The radial field can be expressed by

$$E_{tr}(\mathrm{MV/m}) = 9.06 \times 10^{-15} n_e(\mathrm{cm}^{-3}) r(\mu\mathrm{m}). \tag{6}$$

It reaches 55 GV/m at $r=1$ μm and for an electronic density $n_e = 6 \times 10^{18}$ cm^{-3}. This is five times smaller than the amplitude of the maximum longitudinal field ($mc\omega_p/e$). The increase of n_e results in an increase of the radial field and shorter betatron period. Figure 1 shows the electron trajectory, the variation of the plasma wiggler strength parameter, and the transverse position r for a single electron of initial energy 2.5 MeV propagating along a 550 μm typical accelerating length obtained in our experiment. The initial position r_0 of the electron in the ion cavity is 1 μm from the axis. Increase in electron mass with propagation (longitudinal acceleration) causes both increase in betatron period and decrease in amplitude. K reaches a maximum value close to 3 when the electron has gained its maximum energy (160 MeV). Emission in the x-ray spectral range is then likely to be produced at the end of the acceleration process. The amplitude of the oscillation r is decreased to less than 0.4 μm, more than one-half its original value. In the simulation, the longitudinal field is kept constant. This assumption is correct if the electron beam remains accelerated within less than the dephasing length L_{def} of the plasma cavity, where the electron only feels the accelerating part of the plasma wave. This

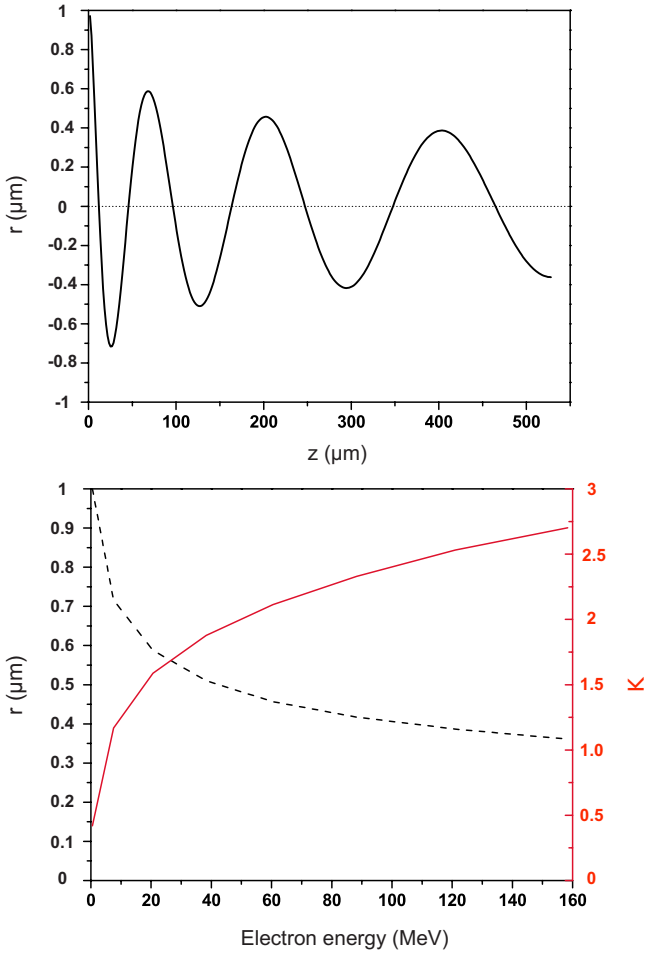

FIG. 1. (Color online) (a) Electron trajectory (Cartesian coordinates) for the case of a single electron with $r_0=1$ μm, and $E_0=2.5$ MeV. The plasma electronic density is $n_e=1\times10^{19}$ cm^{-3}. The electron propagates along the z axis in the transversal plane ($x=r$, $y=0$). (b) Distribution of the plasma wiggler parameters K (dotted line) and r (solid line) generated by the electron trajectory (a).

is the case for the low electronic density of our experimental conditions for which $L_{def}=1.3$ mm. Taking into account the dephasing effect provides a final electron energy decreased by 5% for the parameters used in Fig. 1. This error remains below the resolution of the electron spectrometer used in the experiments and will not affect the x-ray analysis in the determination of r_0.

The parametric dependence of the x-ray spectra on the initial electron oscillation amplitude and on the total acceleration is displayed in Figs. 2 and 3. For these simulations, the electron plasma density is kept constant at $n_e=1\times10^{19}$ cm^{-3} and the electron parameters (energy and r_0) were varied in regard to our experimental conditions. In Fig. 2, electrons are accelerated from 10 to 150 MeV for $r_0=1$ and 3 μm. The x-ray intensity increases up to $\omega \simeq \omega_{pk}$ and then drops exponentially. Both the peak x-ray energy and intensity increase with r_0 as expected from Eqs. (4) and (5). The x-ray intensity distribution is almost flat in the few keV spectral range for $r_0=3$ μm. For $r_0=1$ μm the intensity produced at 3 keV decreases by one-half compared to the maxi-

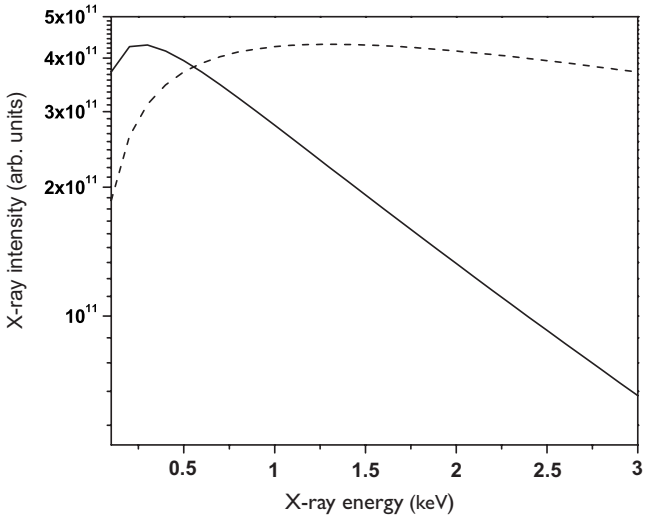

FIG. 2. Theoretical variation of the x-ray spectrum with r_0. solid line: $r_0=1$ μm; dashed line: $r_0=3$ μm. Electrons are accelerated from 10 to 150 MeV.

mum centered at 0.3 keV. Proper accounting of the evolution in electron energy, betatron period, and oscillation amplitude significantly affects the radiation: the x-ray intensity produced by an electron of 120 MeV ($r_0=3$ μm) along its whole trajectory overestimates by a factor of 2 the x-ray intensity per spectral bandwidth as well as the peak x-ray energy compared to the distribution shown in Fig. 2.

The behavior of the x-ray spectrum for electrons accelerated up to 40 and 150 MeV is displayed in Fig. 3. r_0 is equal to 1 μm in each case. The peak x-ray energy varies quadratically with the electron beam energy and the spectrum becomes significantly broader for the more energetic electron case. Electrons accelerated up to 40 MeV do not participate significantly to the x-ray emission in the few keV range.

The x-ray spectrum is as well strongly affected by the decrease of the betatron amplitude and the increase of the

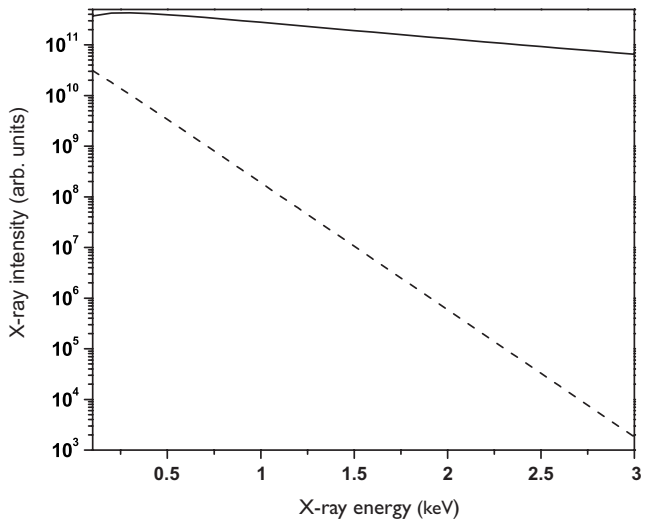

FIG. 3. Theoretical variation of the x-ray spectrum with electron energy ($r_0=1$ μm). Electrons are accelerated from 10 MeV up to 150 MeV (solid line) and up to 40 MeV (dashed line).

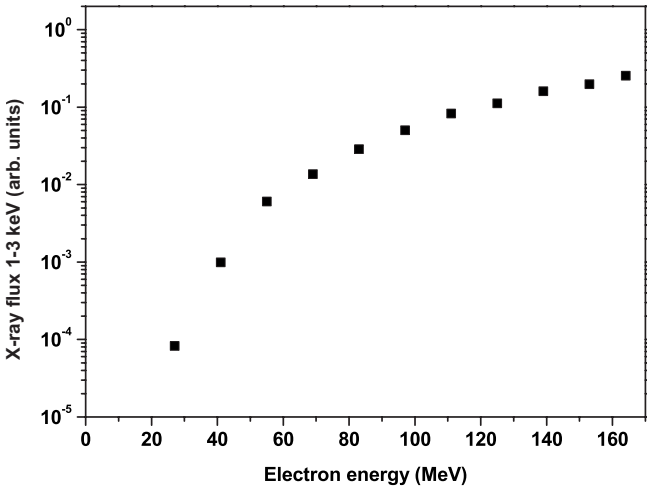

FIG. 4. X-ray intensity generated in the 1–3 keV spectral bandwidth by monoenergetic electrons accelerated from 2.5 MeV to final energies between 27 and 164 MeV. Each electron propagates in the plasma wiggler with the initial conditions: $r_0=3$ μm and $n_e=1\times10^{19}$ cm^{-3}.

oscillation period as the electron accelerates in the cavity. The resulting x-ray wavelength and flux emitted by the electron vary as it propagates, and each electron energy does not participate equally to the overall spectrum. Figure 4 shows the theoretical case of the x-ray intensity generated by monoenergetic electrons of final energies between 27 and 164 MeV. The x-ray flux is integrated within the 1–3 keV spectral range from a single electron accelerated up to its final energy, represented on the x coordinate. Each electron propagates in the plasma wiggler characterized with $E_0=2.5$ MeV, $r_0=3$ μm, and $n_e=1\times10^{19}$ cm^{-3}. We can see that, in this x-ray spectral range, the electrons that produce a significant amount of x-ray radiation have energies larger than 60 MeV. This confirms as well that an electron accelerated in the ion cavity mainly produces keV x rays at the end of the acceleration process and within the very last betatron oscillations. Assuming validity of the single particle model, these strong dependencies of the x-ray spectrum on the electrons properties will allow the direct analysis of K and r from experimentally measured electron and x-ray spectra.

III. EXPERIMENTAL ELECTRON AND X-RAY PROPERTIES

The experiments were performed with the 50 TW laser system at the Laboratoire d'Optique Appliquée [20]. The Ti:Sa produced laser beam has a 40 nm broadband spectrum centered at $\lambda_0=820$ nm. The pulse duration is 30 fs and energies up to 1.5 J can be delivered on target with a linear horizontal polarization. We used a 1 m focal length parabolic mirror to focus the 55 mm diameter laser beam onto the edge of a supersonic Helium gas jet (Fig. 5). The jet profile, which has been fully characterized, shows a uniform and sharp edge density distribution [21]. The laser focal spot has a beam waist w_0 of 18 μm which contains 50% of the total laser energy. This system produces a vacuum focused intensity up

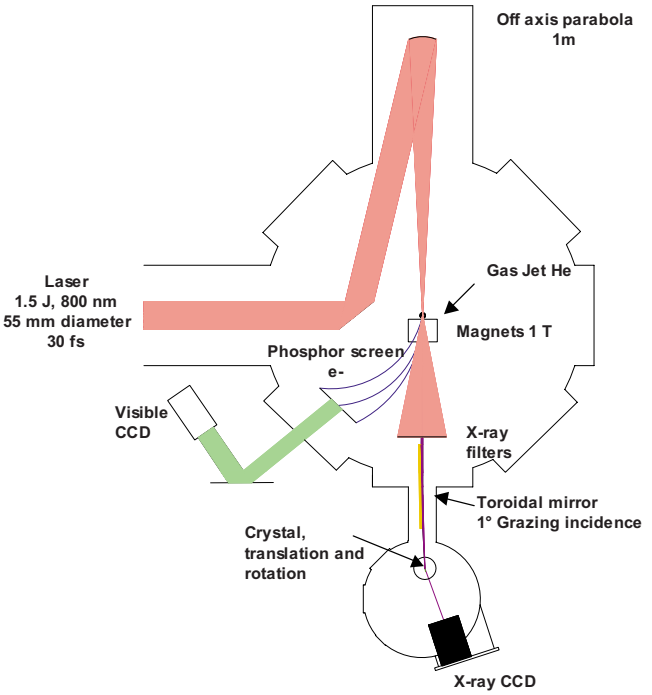

FIG. 5. (Color online) Experimental setup for the x-ray and electron beams' characterization.

to 3×10^{18} W/cm^2, which corresponds to a normalized vector potential a_0 of 1.2. The electron plasma density can be tuned from 10^{18} to 5×10^{19} cm^{-3}.

In the experiment we measured the electrons accelerated above 40 MeV from plasma electronic densities $n_e=6\times10^{18}$ cm^{-3} to $n_e=1.5\times10^{19}$ cm^{-3} by deviating them (with a 1 T permanent magnet) onto a phosphor screen imaged with a visible charge coupled device (CCD) camera. The energies below 40 MeV could not be recorded as the particle deviation was too strong in that case and the electrons were blocked by the magnet. Lesser strength magnets result in excessive noise on the x-ray detector. The resolution of the spectrometer is limited by the dispersing power of the magnet and also by the electron beam spatial quality. For our experimental arrangement, it reaches 17 and 6 MeV for, respectively, 200 and 100 MeV electron energies. The phosphor screen was placed 12 cm away from the magnet and tilted at 45° compared to the laser axis so that electrons up to 200 MeV could potentially be measured. A 100 μm thick aluminum foil was inserted in front of the screen to avoid its direct exposure to the laser light.

The x-ray spectrum was obtained by using a set of diffractive crystals coupled to a toroidal focusing optic. The gold coated 1° grazing incidence toroidal mirror, which has a 20×10 mrad^2 acceptance angle, was placed 50 cm away from the source. It focused the x rays 50 cm further away where a back illuminated x-ray CCD was positioned. Between the mirror and the CCD, x rays from 700 eV to 3.5 keV were diffracted using two different flat crystals: TlAp (thallium acid phtalate, $2d=25.9$ Å) and ADP (ammonium dihydrogen phosphate, $2d=10.648$ Å). The spectrum could not be recorded in a single laser shot as the x-ray monochromator must be tuned to measure each spectral bandwidth.

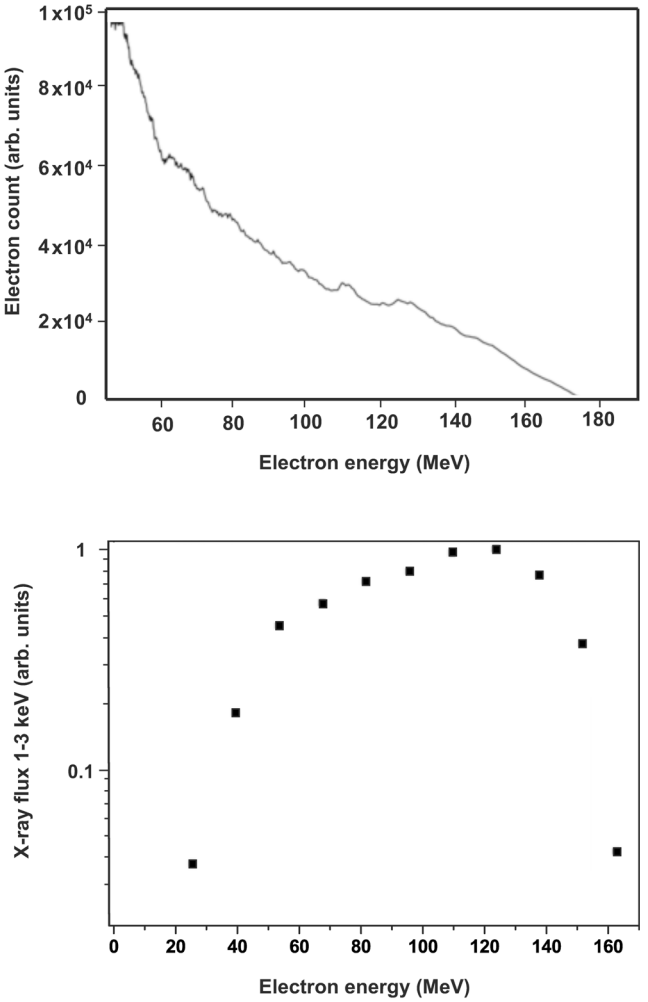

FIG. 6. (Color online) X-ray intensity generated in the 1–3 keV spectral bandwidth as a function of electron energy. The experimental electron distribution used for the simulation is shown. It is averaged over 30 shots. $E_0=2.5$ MeV, $r_0=3$ μm, and $n_e=6\times10^{18}$ cm^{-3}.

All electron spectra considered in the present analysis were obtained in the same regime of wakefield acceleration for which an exponential distribution function of electrons is produced [22]. Occasional shots showing monoenergetic features were not considered. Electrons below 40 MeV were assumed to obey previously measured Maxwellian distribution [22]. Figure 6 shows the calculated integrated x-ray flux within 1–3 keV generated by an experimental electron beam with respect to the electron's final energy. The x-ray flux emitted by the high energy electrons (>130 MeV) drops due to the low charge of the electron beam at high energies. Thus the electronic energy that contributes the most to the x-ray emission in the 1–3 keV spectral range is close to 120 MeV.

IV. CHARACTERIZATION OF THE PLASMA WIGGLER FROM SPECTRAL MEASUREMENTS

In our experimental conditions, the x-ray emission is produced in the plasma wiggler regime ($K\gg1$), where high har-

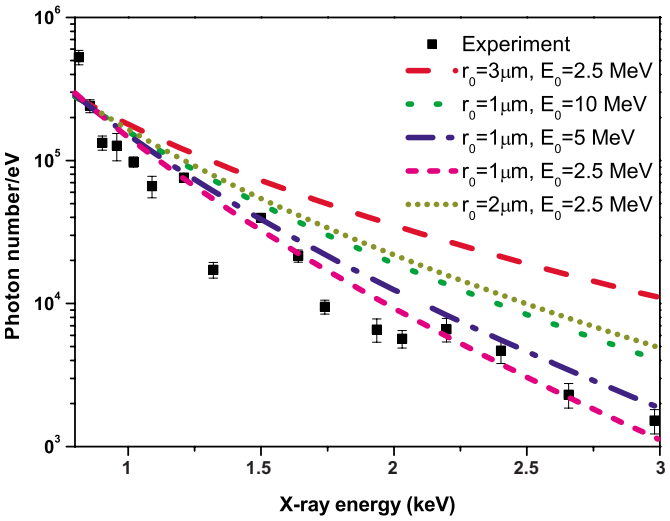

FIG. 7. (Color online) Experimental and calculated x-ray spectra displayed for an electronic density $n_e=6\times10^{18}$ cm^{-3}. Each experimental data point corresponds to an average of ten laser shots. The simulated x-ray spectra is shown for $r_0=1$, 2, and 3 μm and E_0 from 2.5 and 10 MeV before acceleration in the ion channel.

monics are radiated. r is indeed not unique in the ion cavity. Since electrons are accelerated to relativistic energies (up to 180 MeV in our experimental conditions), the effective mass γm increases which results in a reduction of r and of the betatron frequency. Thus a distribution of K and r must be considered as a function of the electron energy rather than constant values. The numerical x-ray spectra are calculated from the measured electron spectra, and initial electron energy and r_0 act as free fitting parameters. Variation in acceleration length accommodates differing electron energies; this corresponds physically to differing injection times of electrons in the wakefield. The relative intensity of the numerical and experimental x-ray spectra are normalized to each other at the lowest x-ray spectral bandwidth.

The use in the analysis of the real electron spectra obtained from the experiment instead of a theoretical maxwellian distribution fitting the data is required to properly determine r_0. As well, since each spectral point corresponds to an average of ten laser shots, the x-ray spectrum is not correlated with a single electron spectrum. Several of those experimental electron spectra were then averaged in the analysis to improve the signal to noise ratio.

Figure 7 shows the experimental x-ray spectra for plasma electron density $n_e=6\times10^{18}$ cm^{-3} and the ones calculated with the code for different values of r_0 and E_0. We can see that the x-ray signal exponentially decays from 1 to 3 keV. The absolute x-ray intensity has been obtained by taking into account the reflectivity of the mirror, the diffraction efficiency of the crystal, as well as the transmission of the Be filter used to block light with energy below 700 eV. The simulated spectra are normalized with respect to the experimental point at 800 eV. The best fit is found for $r_0=1$ μm and $E_0=2.5$ MeV, in agreement with the far field imaging analysis of the x-ray beam [16].

If we increase the value of r_0 and keep the initial electron energy E_0 at 2.5 MeV, the experimental spectrum cannot be fitted properly anymore. With $r_0=2$ μm and $r_0=3$ μm, the simulated spectrum highly overestimates the experimental data. This effect becomes even more important at higher x-ray energies. We also varied the initial electron energy and kept $r_0=1$ μm constant. For $r_0=1$ μm, 5 MeV remains an acceptable value to fit the experimental data, and higher values of the E_0 are no longer valid. This is in agreement with the recent result proposed by Lu *et al.* [23] where $p_0=\omega_0/\sqrt{3}\omega_p$, which in our case means $p_0\simeq10$ ($E_0=5$ MeV). We have found that initial betatron amplitudes below 0.5 μm cannot provide accurate fit of the experimental data with physically meaningful values of E_0. It is very likely that in the conditions of our experiment we are at the boundary between the bubble regime and the forced laser wakefield regime of electron acceleration. By looking separately at all the electron spectra, several (one out of five) have small monoenergetic components. Taken separately, each of these spectra are then likely to generate slightly different x-ray spectra. We estimated the influence of this averaging process by taking into account 10, 20, and 30 spectra in the analysis. The resulting averaged electron spectra have a 100% energy spread and their slope and intensity remain very similar as we increase the number of averaged shots. For $E_0=2.5$ MeV and $r_0=1$ μm accurate fits of the experimental data can be obtained by averaging over at least ten electron spectra, as was done in the present analysis.

V. CONCLUSION AND PERSPECTIVES

We have used the x-ray spectral distribution of the betatron radiation to characterize the initial amplitude oscillation r_0 of the electrons accelerated in the wakefield cavity. The analysis shows that $r_0=1$ μm for our experimental conditions. The possibility in the future to acquire such high resolution spectrum in a single shot and with a spectral bandwidth extended to 10 keV will further improve the determination of r_0. This first spectral analysis of the betatron properties strongly confirms the tiny (close to a micrometer) nature of the transverse electron excursion during its acceleration in the wakefield cavity, as was previously inferred from the spatial x-ray properties [16,17]. The recent promising results on the production of quasimonoenergetic electron beams as well as the development of injection techniques to stabilize the electron beam shot to shot (charge, energy, position) [4–8,24] open the way toward an even more precise correlation between x rays and electrons, and will be a direct probe of the electrostatic fields structure generated in the ion channel produced by laser wakefields. So far, the highest monoenergetic electron beam with our 50 TW laser has been observed at 170 MeV [6] for the same experimental conditions and 250 MeV using the newly demonstrated injection technique [24], and given the efforts that are realized around the world to produce higher energy electron beams, it is likely that intense (nC) electron beams could reach 1 GeV in the very near future. On the other hand, the use of modulated plasma density wakefield cavities [25] or higher power lasers to increase the focal spot size while keeping a_0 constant can both lead to larger K and r_0 values. Hence if we consider a 1 GeV electron beam, with particles

oscillating with betatron amplitudes of 10 μm, K reaches 188 for $n_e = 1 \times 10^{19}$ cm^{-3} and the spectrum peaks at about 600 keV [26]. As the number of photons is proportional to K [14] with $N_x \simeq 5.6 \times 10^{-3} N_0 K$, where N_0 is the number of betatron oscillations undergone by the electron, a factor of 100 can then be gained on the number of photons compared to the present x-ray flux (10^6 photons/shot/0.1% BW). Those perspectives open the way to a series of promising application experiments as the betatron source possesses a time duration that is matched with that of the laser [27], and a perfect synchronization to drive femtosecond pump-probe experiments. Ultrafast x-ray diffraction investigations [28–32] could potentially be extended to ultrafast x-ray absorption with laser-produced plasma radiation sources.

ACKNOWLEDGMENTS

This work was supported by the Agence Nationale de la Recherche: COKER project ANR-06-BLAN-0123-01 and ACCEL1 project NT05-2-41699. F.A. acknowledges useful discussions with the SPL group at LOA for electron beam diagnostics.

[1] T. Tajima and J. M. Dawson, Phys. Rev. Lett. **43**, 267 (1979).
[2] Eric Esarey, Phillip Sprangle, Jonathan Krall, and Antonio Ting, IEEE Trans. Plasma Sci. **24**, 252 (1996).
[3] A. Pukhov and J. Meyer-ter-vehn, Appl. Phys. B: Lasers Opt. **74**, 355 (2002).
[4] S. P. D. Mangles *et al.*, Nature (London) **431**, 535 (2004).
[5] C. G. R. Geddes, Cs. Toth, J. van Tilborg, E. Esarey, C. B. Schroeder, D. Bruhwiler, C. Nieter, J. Cary, and W. P. Leemans, Nature (London) **431**, 538 (2004).
[6] J. Faure, Y. Glinec, A. Pukhov, S. Kiselev, S. Gordienko, E. Lefebvre, J.-P. Rousseau, F. Burgy, and V. Malka, Nature (London) **431**, 541 (2004).
[7] B. Hidding, K. U. Amthor, B. Liesfeld, H. Schwoerer, S. Karsch, M. Geissler, L. Veisz, K. Schmid, J. G. Gallacher, S. P. Jamison, D. Jaroszynski, G. Pretzler, and R. Sauerbrey, Phys. Rev. Lett. **96**, 105004 (2006).
[8] E. Miura, K. Koyama, S. Kato, S. Saito, M. Adachi, Y. Kawada, T. Nakamura, and M. Tanimoto, Appl. Phys. Lett. **86**, 251501 (2005).
[9] A. Rousse *et al.*, Phys. Rev. Lett. **93**, 135005 (2004).
[10] K.-T. Phuoc, F. Burgy, J.-P. Rousseau, V. Malka, A. Rousse, R. Shah, D. Umstadter, A. Pukhov, and S. Kiselev, Phys. Plasmas **12**, 023101 (2005).
[11] D. H. Whittum, Phys. Fluids B **4**, 730 (1992).
[12] S. Kiselev, A. Pukhov, and I. Kostyukov, Phys. Rev. Lett. **93**, 135004 (2004).
[13] E. Esarey, B. A. Shadwick, P. Catravas, and W. P. Leemans, Phys. Rev. E **65**, 056505 (2002).
[14] I. Kostyukov, S. Kiselev, and A. Pukhov, Phys. Plasmas **10**, 4818 (2003).
[15] S. Kneip *et al.*, Phys. Rev. Lett. **100**, 105006 (2008).
[16] K. Ta Phuoc, S. Corde, R. Shah, F. Albert, R. Fitour, J. P. Rousseau, F. Burgy, B. Mercier, and A. Rousse, Phys. Rev. Lett. **97**, 225002 (2006).
[17] R. C. Shah, F. Albert, K. T. Phuoc, O. Shevchenko, D. Boschetto, A. Pukhov, S. Kiselev, F. Burgy, J.-P. Rousseau, and A. Rousse, Phys. Rev. E **74**, 045401(R) (2006).
[18] J. D. Jackson, *Classical Electrodynamics*, 3rd ed. (Wiley, New York, 2001).
[19] J. Schwinger, Phys. Rev. **75**, 1912 (1949).
[20] M. Pittman *et al.*, Appl. Phys. B: Lasers Opt. **74**, 529 (2002).
[21] V. Malka, C. Coulaud, J. P. Geindre, V. Lopez, Z. Najmudin, D. Neely, and F. Amiranoff, Rev. Sci. Instrum. **71**, 2329 (2000).
[22] V. Malka, S. Fritzler, E. Lefebvre, M. M. Aleonard, F. Burgy, J. P. Chambaret, J. F. Chemin, K. Krushelnick, G. Malka, S. P. D. Mangles, Z. Najmudin, M. Pittman, J. P. Rousseau, J. N. Scheurer, B. Walton, and A. E. Dangor, Science **298**, 1596 (2002).
[23] W. Lu, C. Huang, M. Zhou, W. B. Mori, and T. Katsouleas, Phys. Rev. Lett. **96**, 165002 (2006).
[24] J. Faure, C. Rechatin, A. Norlin, A. Lifschitz, Y. Glinec, and V. Malka, Nature (London) **444**, 737 (2006).
[25] K. Ta Phuoc, E. Esarey, V. Leurent, E. Cormier-Michel, C. G. R. Geddes, C. B. Schroeder, A. Rousse, and W. P. Leemans, Phys. Plasmas (to be published).
[26] A. Rousse, K. Ta Phuoc, R. Shah, R. Fitour, and F. Albert, Eur. Phys. J. D **45**, 391 (2007).
[27] Kim Ta Phuoc *et al.*, Phys. Plasmas **14**, 080701 (2007).
[28] C. Rischel, Antoine Rousse, Ingo Uschmann, Pierre-Antoine Albouy, Jean-Paul Geindre, Patrick Audebert, Jean-Claude Gauthier, Eckhart Forster, Jean-Louis Martin, and Andre Antonetti, Nature (London) **390**, 490 (1997).
[29] C. Rose-Petruck, R. Jimenez, T. Guo, A. Cavalleri, C. W. Siders, F. Raksi, J. A. Squier, B. C. Walker, K. R. Wilson, and C. P. J. Barty, Nature (London) **398**, 310 (1999).
[30] C. W. Siders, A. Cavalleri, K. Sokolowski-Tinten, Cs. Tóth, T. Guo, M. Kammler, M. Horn von Hoegen, K. R. Wilson, D. von der Linde, and C. P. J. Barty, Science **286**, 1340 (1999).
[31] A. Rousse, C. Rischel, S. Fourmaux, I. Uschmann, S. Sebban, G. Grillon, Ph. Balcou, E. Förster, J. P. Geindre, P. Audebert, J. C. Gauthier, and D. Hulin, Nature (London) **410**, 65 (2001).
[32] K. Sokolowski-Tinten, C. Blome, J. Blums, A. Cavalleri, C. Dietrich, A. Tarasevitch, I. Uschmann, E. Förster, M. Kammler, M. Horn-von-Hoegen, and D. von der Linde, Nature (London) **422**, 287 (2003).